1   **Ablation of Keratan Sulfate Accelerates Early Phase Pathogenesis of ALS**

2

3   Kenichi Hirano,[1,2,*] Tomohiro Ohgomori,[1,*] Kazuyoshi Kobayashi,[1,2,*] Fumiaki

4   Tanaka,[3] Tomohiro Matsumoto,[1,2] Takamitsu Natori,[4] Yukihiro Matsuyama,[5] Kenji

5   Uchimura,[1] Kazuma Sakamoto,[1] Hideyuki Takeuchi,[6] Akihiro Hirakawa,[7] Akio

6   Suzumura,[6] Gen Sobue,[3] Naoki Ishiguro,[2] Shiro Imagama,[2,**] Kenji Kadomatsu[1,**]

7

8   *These authors contributed equally to this work.

9

10   Departments of [1]Biochemistry, [2]Orthopedics, [3]Neurology and [7]Center for Advanced

11   Medicine and Clinical Research, Nagoya University Graduate School of Medicine,

12   Nagoya 466-8550, Japan; [4]Department of Health and Nutrition, Yamanashi Gakuin

13   University, Kofu 400-8575, Japan; [5] Department of Orthopedics, Hamamatsu University

14   School of Medicine, Hamamatsu 431-3192, Japan; [6]Department of Neuroimmunology,

15   Research Institute of Environmental Medicine, Nagoya University, Nagoya 464-8601,

16   Japan

17

18   **Correspondence should be addressed to Kenji Kadomatsu and Shiro Imagama. Kenji

1   Kadomatsu: Department of Biochemistry, Nagoya University Graduate School of

2   Medicine, Nagoya 466-8550, Japan. E-mail: kkadoma@med.nagoya-u.ac.jp

3   Shiro Imagama: Department of Orthopedics, Nagoya University Graduate School of

4   Medicine, Nagoya 466-8550, Japan. E-mail: imagama@med.nagoya-u.ac.jp

5

6   **Running head:** Keratan sulfate in early phase pathogenesis of ALS

7

8   **Key words:** keratan sulfate; amyotrophic lateral sclerosis; microglia; GlcNAc6ST-1

9

1 **Abstract**

2 Biopolymers consist of three major classes, i.e., polynucleotides (DNA, RNA),

3 polypeptides (proteins) and polysaccharides (sugar chains). It is widely accepted that

4 polynucleotides and polypeptides play fundamental roles in the pathogenesis of

5 neurodegenerative diseases. But, sugar chains have been poorly studied in this process,

6 and their biological/clinical significance remains largely unexplored. Amyotrophic

7 lateral sclerosis (ALS) is a motoneuron-degenerative disease, the pathogenesis of which

8 requires both cell autonomous and non-cell autonomous processes. Here, we

9 investigated the role of keratan sulfate (KS), a sulfated long sugar chain of proteoglycan,

10 in ALS pathogenesis. We employed ALS model SOD1^{G93A} mice and GlcNAc6ST-1$^{-/-}$

11 mice, which are KS-deficient in the central nervous system. Unexpectedly,

12 SOD1^{G93A}GlcNAc6ST-1$^{-/-}$ mice exhibited a significantly shorter lifespan than SOD1^{G93A}

13 mice and an accelerated appearance of clinical symptoms (body weight loss and

14 decreased rotarod performance). KS expression was induced exclusively in a

15 subpopulation of microglia in SOD1^{G93A} mice, and became detectable around

16 motoneurons in the ventral horn during the early disease phase before body weight loss.

17 During this phase, the expression of M2 microglia markers was transiently enhanced in

18 SOD1^{G93A} mice, while this enhancement was attenuated in SOD1^{G93A}GlcNAc6ST-1$^{-/-}$

3

1   mice. Consistent with this, M2 microglia were markedly less during the early disease

2   phase in SOD1^{G93A}GlcNAc6ST-1$^{-/-}$ mice. Moreover, KS expression in microglia was

3   also detected in some human ALS cases. This study suggests that KS plays an

4   indispensable, suppressive role in the early phase pathogenesis of ALS and may

5   represent a new target for therapeutic intervention.

1 **Introduction**

2 Amyotrophic lateral sclerosis (ALS) is a life-threatening neurodegenerative disease

3 specific to upper and lower motoneurons. Extensive studies on ALS models have

4 revealed that both cell-autonomous and non-cell-autonomous mechanisms are required

5 for the onset and progression of this disease [1-4]. Among non-cell-autonomous

6 mechanisms, microglia are thought to be important for the progression [2]. Although

7 many important proteins, such as superoxide dismutase 1 (SOD1), TDP43, FUS/TLS,

8 C9ORF72, profilin 1 and optineurin, have been identified [5], the pathogenesis of ALS

9 is not fully understood, and the development of preventive and/or therapeutic measures

10 for this disease is still an unmet goal. In particular, the significance of sugar chains has

11 been little studied in this disease.

12 Although there is still debate in regard to the proper categorization of microglia,

13 it is widely accepted that activated microglia exert dual functions, i.e., pro-inflammatory

14 and anti-inflammatory functions [6]. Accordingly, activated microglia are sometimes

15 categorized as M1 or M2 microglia. Thus, upon activation, M1 microglia express

16 pro-inflammatory molecules, such as NOX2, IL-1β and TNFα, as well as cell surface

17 markers, including CD86 [7-9]. On the other hand, M2 microglia express a different set

18 of cytokines and molecular markers that are associated with anti-inflammatory functions,

1 and which include IL-4, CD206, Ym1 and arginase1 [7, 8, 10, 11]. Although this

2 categorization might be an oversimplification, the *in vivo* status of activated microglia is

3 probably on a continuum between these two extreme states. Thus, microglia can be

4 polarized into an activation state that is intermediate between a pro-inflammatory and an

5 anti-inflammatory state.

6 Chondroitin sulfate (CS), a long sugar chain (named glycosaminoglycan) of

7 proteoglycans, functions as a potent inhibitor for axonal regeneration/sprouting and

8 synaptic plasticity [12, 13]. Keratan sulfate (KS) is another glycosaminoglycan, and is

9 recognized by the KS-specific antibody 5D4. KS is composed of repeating disaccharide

10 units of 3Galβ1–4GlcNAcβ1, where the C6 position of the GlcNAc residue is always

11 sulfated, while that of Gal is sometimes sulfated. GlcNAc6ST-1 mediates sulfation of

12 GlcNAc, which is an essential step for KS biosynthesis [14]. Therefore,

13 GlcNAc6ST-1-deficient (GlcNAc6ST-1$^{-/-}$) mice show loss of KS in the central nervous

14 system (CNS) [15]. Interestingly, this loss seems to be specific to the CNS, since other

15 organs such as cornea and cartilage express KS in GlcNAc6ST-1$^{-/-}$ mice [15, Uchimura

16 et al., unpublished data]. We recently found that 5D4-reactive KS inhibits axonal

17 regeneration/sprouting, and its inhibitory activity is as strong as that of CS [16, 17]. On

18 the other hand, the roles of glycosaminoglycans in neurodegenerative diseases have

1   been little studied. Here, we demonstrate an unexpected role of KS in the early phase

2   pathogenesis of ALS.

3

1 **Results**

2 **KS was induced in the spinal cord of SOD1^{G93A} mice**

3 To investigate the biological significance of KS in ALS, we employed ALS model

4 SOD1^{G93A} mice. SOD1^{G93A} mice in the end stage (24 weeks after birth) and their

5 age-matched non-Tg littermates were compared for KS expression by immunoblot

6 analysis using the KS-specific antibody 5D4. KS was not expressed in the lumbar spinal

7 cords of non-Tg mice, but was remarkably induced in SOD1^{G93A} mice (Figure 1A). As

8 KS is a long sugar chain, KS-bearing proteoglycans appear as smear bands in

9 immunoblots, as shown in Figure 1A. Immunohistochemical analysis confirmed that KS

10 expression was strikingly induced and distributed throughout the whole area,

11 particularly in the gray matter, in SOD1^{G93A} mice (Figure 1B).

12

13 **KS expression began in the early phase of disease before body weight loss**

14 SOD1^{G93A} mice began to lose body weight around 120 days (17-18 weeks) after birth

15 (data not shown). Diseased mice progressively manifested motor paralysis, and reached

16 the end stage at around 24 weeks. It is important to determine when KS starts to emerge

17 in relation to the progression of disease. To this end, we examined the time course of KS

18 expression.

1   An apparent expression was detected at 18 weeks in the lumbar spinal cord of

2   SOD1^{G93A} mice in immunoblot analysis, although a faint expression of KS was detected

3   at 12 weeks (Figure 2A). The expression increased along with the disease progression

4   (Figure 2A). Notably, immunohistochemical analysis revealed that KS was expressed at

5   12 weeks in the ventral horn of the spinal cord (Figure 2B, arrows), where motoneurons

6   exist. Thereafter, the distribution of expression expanded throughout the whole area of

7   the spinal cord (Figure 1B). Therefore, the fact that only a faint band was detected at 12

8   weeks in the immunoblotting analysis was probably due to the restricted localization of

9   KS expression at this stage.

10

11   **A subpopulation of microglia expressed KS**

12   To determine which cells expressed KS, double immunofluorescence was performed for

13   KS and cell-specific markers on the lumbar spinal cord of SOD1^{G93A} mice at 18 weeks.

14   Colocalization was observed in a subpopulation of Iba1-positive cells (microglia), i.e.,

15   both KS-positive and KS–negative cells were found among the Iba1-positive cells

16   (Figure 3A-C). In contrast, no colocalization was detected with glial fibrillary acidic

17   protein (GFAP) (astrocyte; Figure 3D-F), NG2 (oligodendrocyte precursor cell; Figure

18   3G-I), or MAP2 (neuron) (data not shown). These data suggested that a subpopulation

1   of microglia expressed KS.

2   We also enriched microglia from the spinal cords of mice at 24 weeks with

3   CD11b affinity beads, and examined their KS expression. The intensity of KS was

4   significantly increased in microglia from $SOD1^{G93A}$ mice as compared with those from

5   non-Tg mice (Figure 3J, K). This enhanced expression of KS in microglia might have

6   been associated with an increased expression of enzymes for KS biosynthesis. To

7   address this question, we next examined the expression levels of these enzymes. The

8   biosynthesis of KS is accomplished through sequential reactions mediated by the

9   enzymes shown in Figure 3L. mRNA expression of these enzymes in the lumbar spinal

10   cord was examined by quantitative RT-PCR for $SOD1^{G93A}$ and age-matched non-Tg

11   mice at 24 weeks. Indeed, a significant increase in mRNA expression was detected for

12   β3GlcNAcT-7, GlcNAc6ST-2, and KSGal6ST in $SOD1^{G93A}$ mice (Figure 3M). Together,

13   these results support the idea that individual microglial cells increase KS production in

14   $SOD1^{G93A}$ mice.

15

16   **KS expression was detected in human ALS**

17   We next asked whether KS might also be expressed in human ALS. To answer this

18   question, we selected human ALS frozen specimens which showed appropriate Iba1

1   staining. Notably, we found KS expression in microglia in 5 cases (2 cases of familial

2   ALS and 3 cases of sporadic ALS). This may partly support the idea that our findings in

3   mouse models could be relevant to human ALS, although further large scale clinical

4   studies are needed to evaluate the significance of KS expression in human ALS. A

5   representative case of familial ALS is shown in Figure 4A-D, and the information of

6   human ALS samples is shown in Figure 4E.

7

8   **Ablation of KS expression in microglia accelerated the pathogenesis of ALS in a**

9   **mouse model**

10   The finding that KS was expressed in microglia in both human and mouse ALS

11   prompted us to ask whether KS had a biological role. Because the loss of KS in

12   GlcNAc6ST-1$^{-/-}$ mice is seen in the CNS [15, Uchimura et al., unpublished data],

13   SOD1^{G93A}GlcNAc6ST-1$^{-/-}$ mice are thought to be a suitable model to investigate the role

14   of KS in ALS. Based on this idea, we generated SOD1^{G93A}GlcNAc6ST-1$^{-/-}$ mice, and

15   compared their phenotype with that of SOD1^{G93A} mice. As expected, KS was not

16   expressed in the spinal cords of SOD1^{G93A}GlcNAc6ST-1$^{-/-}$ mice (Figure 5A, B).

17   Nevertheless, the microglia increased in number in the spinal cord to a similar extent in

18   both SOD1^{G93A}GlcNAc6ST-1$^{-/-}$ and SOD1^{G93A} mice at 24 weeks (Figure 5C-E).

1   To our surprise, a significant difference in lifespan was observed between these

2   two genotypes. Lifespan was significantly decreased in SOD1^{G93A}GlcNAc6ST-1$^{-/-}$ mice

3   (Figure 6A). Appearance of body weight loss was also accelerated in

4   SOD1^{G93A}GlcNAc6ST-1$^{-/-}$ mice (Figure 6B). A decrease in rotarod performance at 15

5   rpm and 20 rpm also occurred earlier in SOD1^{G93A}GlcNAc6ST-1$^{-/-}$ mice (Figure 6C, D).

6   Thus, ablation of KS in microglia resulted in acceleration of appearance of clinical

7   symptoms and consequently shortened the lifespan in the mouse ALS model.

8

9   **KS-positive microglia consisted of CD86-positive and -negative cells**

10   To investigate the mechanism underlying the shortened lifespan of

11   SOD1^{G93A}GlcNAc6ST-1$^{-/-}$ mice, we further characterized KS-positive microglia. We

12   compared the spatio-temporal expression of KS and CD86, a representative marker for

13   M1 microglia, in SOD1^{G93A} mice at the early (12 weeks), body weight loss (18 weeks)

14   and disease end stage (24 weeks) phases. KS began to be expressed at 12 weeks (Figure

15   7A). At this phase, although both KS$^+$CD86$^-$ and KS$^+$CD86$^+$ microglia existed,

16   KS$^+$CD86$^-$ microglia were the major population in SOD1^{G93A} mice (Figure 7A-D). The

17   proportion of KS$^+$CD86$^+$ microglia increased with disease progression, but KS$^+$CD86$^-$

18   microglia still existed (Figure 7E-K). Flow cytometric analysis for microglia, which

12

1 were enriched by CD11b affinity beads from mice at 24 weeks, revealed that the

2 numbers of both $CD86^+$ and $CD86^-$ cells were increased in $SOD1^{G93A}$ mice (Figure 7L).

3 Most of the $CD86^+$ cells were KS^+, while a significant portion of the $CD86^-$ cells were

4 KS^+ (Figure 7M). Thus, the population of KS^+CD86^- microglia was comparable with

5 that of KS^+CD86^+ microglia in $SOD1^{G93A}$ mice at 24 weeks (Figure 7M).

6

7 **The transient enhancement of M2 markers was diminished in**

8 **$SOD1^{G93A}GlcNAc6ST-1^{-/-}$ mice**

9 Considering that the KS-positive microglia consisted of CD86-positive and -negative

10 cells, we next examined the temporal expression profiles of M1 and M2 markers in the

11 spinal cord. Expression of the M1 markers CD86, IL-1β, TNF-α, and NOX2 was

12 steadily increased as the disease progressed (Figure 8A-D). There was no difference in

13 M1 marker expression between $SOD1^{G93A}$ and $SOD1^{G93A}GlcNAc6ST-1^{-/-}$ mice (Figure

14 8A-D).

15   In contrast, the expression profiles of the M2 markers CD206, arginase1, Ym1

16 and IL-4 were significantly different between $SOD1^{G93A}$ and $SOD1^{G93A}GlcNAc6ST-1^{-/-}$

17 mice based on a statistical analysis with two-way ANOVA (Figure 8E-H). Thus, the

18 expressions of these genes were transiently enhanced at 12-15 weeks of age in

1 SOD1^{G93A} mice (Figure 8E-H). This is the early phase before body weight loss, when

2 KS began to be expressed in microglia (Figure 2). Notably, this enhancement of M2

3 marker expression observed in SOD1^{G93A} mice was strikingly attenuated in

4 SOD1^{G93A}GlcNAc6ST-1$^{-/-}$ mice (Figure 8E-H).

5   We next examined the fate of M1 and M2 microglia during progression of the

6 disease. M1 microglia (CD86-positive) consistently increased in number as the disease

7 progressed from 12 weeks to 24 weeks in both SOD^{G93A} mice and

8 SOD^{G93A}GlcNAc6ST-1$^{-/-}$ mice (Figure 7 and 9). In contrast, M2 microglia

9 (CD206-positive) were abundant at 15 weeks and were continuously detectable until 24

10 weeks in SOD^{G93A} mice, whereas SOD^{G93A}GlcNAc6ST-1$^{-/-}$ mice showed markedly less

11 M2 microglia at 15 weeks (Figure 10). These profiles were almost consistent with those

12 of marker expression shown in Figure 8.

13   As a majority of KS-positive microglia were CD86-negative at 12 weeks

14 (Figure 7A-D), these KS^{+}CD86^{-} microglia could be a major source of future polarized

15 cells. We asked if KS^{+}CD86^{-} microglia were M2 microglia (CD206-positive) at 15

16 weeks. Immunohistochemical analysis using sequential thin sections revealed that

17 KS^{+}CD86^{-} microglia did not express CD206 at 15 weeks, while CD206-positive cells

18 were KS-negative (Figure 11). Our data collectively suggest that KS^{+}CD86^{-} microglia

1   could be directly polarized to KS^-CD206^+ microglia or indirectly influence the

2   polarization of other types of cells to KS^-CD206^+ microglia as the disease progresses,

3   although other pathways of M2 polarization cannot be excluded.

4

1　**Discussion**

2　Striking progress has been made in our understanding of neurobiology in the last several

3　decades. Most of the advances have been realized by focusing on proteins as the main

4　players in neurobiological mechanisms. However, considering that biopolymers consist

5　of three main classes, i.e., polynucleotides (DNA and RNA), polypeptides (proteins)

6　and polysaccharides (sugar chains), important biological functions are also expected to

7　be attributable to sugar chains. In addition, most proteins are modified with sugar chains.

8　It has recently been accepted that CS is a potent inhibitor of axonal

9　regeneration/sprouting and synaptic plasticity [12, 13], and several candidate receptors

10　for CS, such as PTPσ and Nogo receptor 1 and 3, have been postulated [18, 19].

11　Although these findings have promoted the emerging research area of

12　glyco-neurobiology, the roles of sugar chains in the nervous system remain largely

13　unknown. The present study is the first to demonstrate an indispensable role of a sugar

14　chain in the pathogenesis of a neurodegenerative disease.

15　　　　We found in the current study that KS-positive microglia progressively expand

16　in SOD1^{G93A} mice (Figure 2). Based on this observation, we initially expected that

17　SOD1^{G93A}GlcNAc6ST-1$^{-/-}$ mice might show a less lethal phenotype compared to

18　SOD1^{G93A} mice. However, we found that the ablation of KS in microglia resulted in

16

1 acceleration of clinical symptoms (body weight loss and decreased rotarod

2 performance) and consequently shortened the lifespan (Figure 6). This phenotype is

3 associated with the attenuation of the transient upregulation of M2 microglia markers,

4 e.g., arginase 1, CD206, Ym1 and IL-4, during the early disease phase (12-15 weeks)

5 before body weight loss in SOD1^{G93A}GlcNAc6ST-1$^{-/-}$ mice (Figure 8). Considering that

6 these M2 markers are reported to be closely associated with anti-inflammatory functions

7 [7, 8, 10, 11], our data collectively suggest that KS plays an indispensable, suppressive

8 role in the early phase pathogenesis of ALS. Furthermore, consistent with the profiles of

9 marker expression, M2 microglia (CD206-positive) are markedly less during the early

10 disease phase in SOD1^{G93A}GlcNAc6ST-1$^{-/-}$ mice compared with SOD1^{G93A} mice, while

11 the consistent increase of M1 microglia (CD86-positive) is comparable in these two

12 genotypes (Figure 7, 9, 10). As a majority of KS-positive microglia are CD86-negative

13 (KS^{+}CD86^{-} microglia) during the early disease phase, these microglia probably play an

14 indispensable role (Figure 7). Although it is speculated that the suppressive role of KS

15 in the early pathogenesis is mediated through the promotion of microglia polarization to

16 an anti-inflammatory state, there might be other possibilities, e.g., the KS expressed by

17 microglia might influence the functions of other cell types.

18   Our study raises the question of whether the function of KS can be generalized

1   to that of other glycosaminoglycans, such as CS, in the pathogenesis of

2   neurodegenerative diseases. There have been only a few reports in this field.

3   Chondroitin sulfate proteoglycans (CSPGs) (i.e., neurocan, versican, phosphacan, and

4   decorin) accumulate in the microenvironment of spinal motoneurons in ALS transgenic

5   rats [20, 21]. These CSPGs are mainly produced by activated astrocytes, but their

6   function is unclear. Our current study highlighted the importance of KS expressed in a

7   subpopulation of microglia. With regard to microglia polarization, it is interesting that

8   microglia/macrophages are activated by CSPGs located in the glial scar after neuronal

9   injury, and polarized into a beneficial state which produces IGF-1 and BDNF [22, 23].

10 Verification of molecular interactions involving KS and CS may shed light on the

11 pathogenesis of ALS and other neurodegenerative diseases. In addition, because the

12 expression of KS synthesis enzymes is concomitantly upregulated (Figure 3), studies on

13 the regulatory mechanism of the expression of these enzymes may provide clues to

14 effective therapy or diagnostic methods for ALS.

1   **Materials and Methods**

2   **Mice**

3   The animal experiments described in this article were performed in accordance with

4   protocols approved by the Animal Care and Use Committee of Nagoya University

5   Graduate School of Medicine. All animals were treated and cared for in accordance with

6   the Nagoya University School of Medicine Guidelines pertaining to the treatment of

7   experimental animals. SOD1^{G93A} transgenic mice, which carry the G93A mutant form of

8   the human SOD1 (B6.Cg-Tg [SOD1-G93A] 1Gur/J line), were purchased from the

9   Jackson Laboratory. Maintenance of these mice and their genotyping were done as

10   described previously [24]. GlcNAc6ST-1$^{-/-}$ mice were produced using D3 embryonic

11   stem cells and ordinary gene-targeting as described previously [14]. GlcNAc6ST-1$^{+/-}$

12   mice obtained after backcrossing with C57BL/6J for more than 11 generations were

13   interbred and these mice were used for mating. The sequences of the primers used for

14   genotyping are listed in Table 1.

15

16   **Human ALS samples**

17   Specimens of lumbar spinal cord (L4-L5 segments) from ALS cases were obtained.

18   Among the specimens examined, those with preserved expression of Iba1 (2 familial

19

1 and 3 sporadic ALS cases) were subjected to further evaluation of KS expression. The

2 diagnosis of ALS was confirmed by the El Escorial diagnostic criteria published by the

3 World Federation of Neurology and by histopathologic findings, particularly the

4 presence of Bunina bodies. The molecular diagnosis was negative for SOD1, FUS/TLS,

5 TDP-43 and OPTN in familial ALS cases. The collection of autopsied human tissues,

6 their use for this study, and consent procedure were approved by the Ethics Committee

7 of Nagoya University Graduate School of Medicine, and written informed consent was

8 obtained from the patients' next-of-kin.

9

10 **Lifespan experiments**

11 Mice were observed daily for survival. An investigator who was blinded to the genotype

12 of mice measured the body weight and motor performance. Both measurements were

13 started at the age of 60 days, and the body weight of mice was measured every 5 days.

14 Testing of motor function using a Rota-rod Treadmill for mice (MK-610A; Muromachi,)

15 was performed once a week. Each weekly session consisted of three trials on the

16 constantly rotating setting at a speed of 15 and 20 rpm. The time remaining on the rotor

17 during a 3 min period was recorded. Mice were judged to have failed the test when, on

18 average in three separate trials, they fell off the rotarod before 2 min. Time of disease

1   onset was retrospectively determined as the time when mice reached peak body weight

2   or the time when mice began to fail the rotarod test. The time of end stage was

3   determined by paralysis so severe that the animal could not right itself within 20

4   seconds when placed on its side, an endpoint frequently used for SOD1

5   mutant-expressing mice [25]. Lifespan was defined by the duration between the birth

6   and the end stage.

7

8   **Immunohistochemistry**

9   Mice were deeply anesthetized with diethylether and transcardially perfused with

10   phosphate buffered saline (PBS) followed by 4% paraformaldehyde (PFA) in 0.1M

11   phosphate buffer (Wako). Isolated lumbar spinal cords were fixed with 4% PFA

12   overnight at 4°C, and cryoprotected by 20% sucrose in 0.1M phosphate buffer at 4°C

13   during the subsequent night. The tissue samples were embedded in Tissue-Tek O.C.T.

14   compound (Sakura Finetek) and quickly frozen by liquid nitrogen. Frozen tissues were

15   cut into 10 μm sections on a cryostat (CM1800; Leica Instruments) and collected on

16   MAS-coated glass slides (Superfrost; Matsunami Glass).

17   The sections were washed in PBS. After blocking with 3% bovine serum

18   albumin (BSA) in PBS containing 0.1% Triton X-100 for 30 min at room temperature,

1 the sections were incubated at 4°C overnight with the following primary antibodies:

2 mouse anti-KS (1:500, clone 5D4; Seikagaku Corporation), rabbit anti-Iba1 (1:500;

3 Wako), rabbit anti-GFAP (1:1000; Sigma), rabbit anti-NG2 (1:500; Millipore), rat

4 anti-CD86 (1:200; BD Biosciences), and rat anti-CD206 (1:200; AbD Serotec). After

5 three rinses with PBS, the sections were incubated for 60 min at room temperature with

6 the following secondary antibodies: AlexaFluor 594 conjugated anti-mouse IgG

7 (Invitrogen), AlexaFluor 488 conjugated anti-rabbit IgG (Invitrogen), AlexaFluor 488

8 conjugated Donkey anti-mouse IgG (Invitrogen), AlexaFluor 594 conjugated Donkey

9 anti-rat IgG (Invitrogen), and AlexaFluor 647 conjugated Donkey anti-rabbit IgG

10 (Invitrogen). For paraffin sections, isolated lumbar spinal cords were fixed with 4% PFA

11 overnight at 4°C, dehydrated with 70% ethanol, and embedded in paraffin. These tissues

12 were cut into 5 μm sections. Immunohistochemistry analysis was performed using a

13 Ventana DISCOVERY system (Ventana Medical Systems). Sections were incubated

14 overnight at 4°C with the following antibodies: mouse anti-KS (1:500; clone 5D4), and

15 rabbit anti-Iba1 (1:500). After three rinses with PBS, the sections were incubated with

16 horseradish peroxidase (HRP)-conjugated secondary antibodies (1:5000; Jackson

17 ImmunoResearch). Binding antibodies were visualized by using a Ventana DAB Map

18 kit (Ventana Medical Systems).

1

SDS-PAGE and Immunoblotting

Mice were deeply anesthetized with diethylether and perfused transcardially with PBS. Each isolated lumbar spinal cord was homogenized in lysis buffer (1% Triton X-100 and 1% protease inhibitor cocktail (Nacalai Tesque) in PBS) for 60 sec at 4°C. The homogenates were centrifuged at $20000 \times g$ for 15 min, and the concentration of the soluble proteins was measured by Bradford protein assay using a Protein Quantification Kit (Dojindo). The soluble proteins were digested with protease-free chondroitinase ABC (1 U/ml; Seikagaku Corporation) in 50 mM Tris-acetate buffer (pH 8.0) for 2 hr at 37°C. The digested and non-digested samples were mixed with $4 \times$ loading buffer (0.25 M Tris-HCl, 20% mercaptoethanol, 8% SDS, 20% sucrose, 0.008% bromophenol blue; pH 6.8) and boiled for 5 min. SDS-PAGE was performed in 6% and 15% gels. After transferring the proteins to a polyvinylidene difluoride (PVDF) membrane (Hybond-P; GE Healthcare) and blocking it with PBS-T containing 5% skim milk for 1 hr at room temperature, the membranes were incubated with mouse anti-KS (1:2000; clone 5D4), rabbit anti-Iba1 (1:1000; Wako), and mouse anti-β-actin (1:10000; Sigma). After three washes with 5% skim milk in PBS-T, the membranes were incubated with the HRP-conjugated secondary antibodies for 30 min at room temperature. Binding

23

1   antibodies were visualized by an ECL Plus kit (GE Healthcare).

2

3   **Quantitative RT-PCR**

4   Total RNA was extracted from the lumbar spinal cords using an RNeasy Lipid Tissue kit

5   (Qiagen) according to the manufacturer's recommendations. The cDNA was prepared

6   from 1 μg of total RNA by using a Transcriptor First Strand cDNA Synthesis Kit

7   (Roche) following the standard protocols. Quantitative PCR was performed on a

8   StepOne (Applied Biosystems) or Mx3000P (Agilent Technologies) using Taqman

9   Probes or SYBR Green (Agilent Technologies), respectively. Samples were subjected to

10   40 cycles of amplification at 95°C for 15 sec and 60°C for 1 min, after holding at 50°C

11   for 2 min and 95°C for 10 min. Relative expression was calculated using the $2^{-(Ct}$

12 $^{\text{experimental sample – Ct internal control sample (GAPDH))}}$ method. The Taqman probes used for the

13   quantitative RT-PCR of KS synthesis enzymes were as follows; Mm00507533_m1,

14   Mm00490018_g1,   Mm00488783_s1,   Mm00517342_m1,   Mm00491466_m1,

15   Mm00480087_m1, and Mm00517855_m1. The sequences of primers used for the

16   quantitative RT-PCR of M1 and M2 markers are listed in Table 2.

17

18   **Flow cytometry**

1   The spinal cords obtained from non-Tg and SOD1^{G93A} mice at 24 weeks were

2   dissociated with 5 mg/ml collagenase in HBSS at 37°C for 45 min, and filtered by using

3   70 µm cell strainers. Immune cells were separated by centrifugation using 38% Percoll

4   in PBS at $2000 \times g$ for 20 min. The immune cells were then suspended with PBS

5   containing 0.5% BSA and 2 mM EDTA and incubated with CD11b magnetic beads

6   (Milteny Biotec GmbH) at 4°C for 15 min. Fcγ receptors on CD11b-enriched cells were

7   blocked by incubation with anti-CD16/CD32 antibody (1:400; BD Biosciences) at 4°C

8   for 15 min. Then, the cells were stained by PE-Cy^{TM}7 conjugated anti-CD86 antibody

9   (2 µg/sample; BD Biosciences) and anti-KS antibody (2 µg/sample) which was labeled

10 with a Zenon Alexa 405 mouse IgG1 labeling kit (Invitrogen) at 4°C for 30 min, and

11 analyzed with FACS Canto II, FACSDiva (Becton Dickinson) and FlowJo (Tree Star).

12

13 **Statistical analysis**

14 An unpaired Student's two-tailed *t*-test was used for analyzing the mRNA expression of

15 the KS synthesis enzymes. The Kaplan Meier method (log-rank test) was used for

16 comparing the lifespan and disease onset of mice of each genotype. Mann Whitney's U

17 test was used for analyzing disease duration. Two-way ANOVA was used to evaluate the

18 difference in the time course of M1 and M2 markers between two groups. We

1 subsequently performed the unpaired Student's two tailed t-test at each week. In all

2 statistical analyses, values of $p < 0.05$ were considered to indicate significance. The

3 statistical analysis was performed using SAS 9.3 (SAS Institute Inc.) and SPSS (SPSS

4 Inc.) software. The investigators performing the statistical analyses were blinded to the

5 group assignments in all procedures.

6

12

13   **Abbreviations**

14   ALS, amyotrophic lateral sclerosis; BSA, bovine serum albumin; CNS, central nervous

15   system; CS, chondroitin sulfate; GFAP, glial fibrillary acidic protein; HRP, horseradish

16   peroxidase; KS, keratan sulfate; PBS, phosphate buffered saline; PFA,

17   paraformaldehyde; PG, proteoglycan; SOD1, superoxide dismutase 1

18

1 **Author contributions**

2 The author(s) have made the following declarations about their contributions:

3 K. Hirano, T. Ohgomori, K. Kobayashi, T. Matsumoto, T. Natori, K. Uchimura and K.

4 Sakamoto performed experiments. H. Takeuchi and A. Suzumura provided animals and

5 supervised animal experiments. F. Tanaka and G. Sobue supervised analysis of human

6 samples. K. Hirano, T. Ohgomori, K. Kobayashi, T. Matsumoto, T. Natori, K. Uchimura

7 and K. Sakamoto and A. Hirakawa performed data analysis. K. Hirano, Y. Matsuyama,

8 N. Ishiguro, S. Imagama and K. Kadomatsu designed the study. K. Hirano, T.

9 Ohgomori, S. Imagama and K. Kadomatsu wrote the manuscript. All authors read and

10 proved the final manuscript.

11

12

1 **References**

2 1. Clement AM, Nguyen MD, Roberts EA, Garcia ML, Boillée, Rule M, McMahon AP,
3 Doucette W, Siwek D, Ferrante RJ, Brown RH Jr., Julien JP, Goldstein LSB, Cleveland
4 DW (2003) Wild-Type nonneuronal cells extend survival of SOD1 mutant motor
5 neurons in ALS mice. Science 302:113-117.

6

7 2. Boillée S, Yamanaka K, Lobsiger CS, Copeland NG, Jenkins NA, Kassiotis G,
8 Kollias G, Cleveland DW (2006) Onset and progression in inherited ALS determined by
9 motor neurons and microglia. Science 312:1389-1392.

10

11 3. Yamanaka K, Chun SJ, Boillee S, Fujimori-Tonou N, Yamashita H, Gutmann DH,
12 Takahashi R, Misawa H, Cleveland DW (2008) Astrocytes as determinants of disease
13 progression in inherited amyotrophic lateral sclerosis. Nat Neurosci 11:251-253.

14

15 4. Yamanaka K, Boillee S, Roberts EA, Garcia ML, McAlonis-Downes M, Mikse OR,
16 Cleveland DW, Goldstein LS (2008) Mutant SOD1 in cell types other than motor
17 neurons and oligodendrocytes accelerates onset of disease in ALS mice. Proc Natl Acad
18 Sci U S A 105:7594-7599.

19

20 5. Ince PG, Highley JR, Kirby J, Wharton SB, Takahashi H, Strong MJ, Shaw PJ.
21 Molecular pathology and genetic advances in amyotrophic lateral sclerosis: an emerging
22 molecular pathway and the significance of glial pathology (2011) Acta Neuropathol
23 122:657-671.

24

25 6. Henkel JS, Beers DR, Zhao W, Appel SH (2009) Microglia in ALS: the good, the bad,
26 and the resting. J Neuroimmune Pharmacol 4:389-398.

27

28 7. Liao B, Zhao W, Beers DR, Henkel JS, Appel SH (2012) Transformation from a
29 neuroprotective to a neurotoxic microglial phenotype in a mouse model of ALS. Exp
30 Neurol 237:147-152.

31

32 8. Kigerl KA, Gensel JC, Ankeny DP, Alexander JK, Donnelly DJ, Popovich PG (2009)
33 Identification of two distinct macrophage subsets with divergent effects causing either
34 neurotoxicity or regeneration in the injured mouse spinal cord. J Neurosci
35 29:13435-13444.

1

9. Meissner F, Molawi K, Zychlinsky A (2010) Mutant superoxide dismutase 1-induced IL-1beta accelerates ALS pathogenesis. Proc Natl Acad Sci U S A 107:13046-13050.

10. David S, Kroner A (2011) Repertoire of microglial and macrophage responses after spinal cord injury. Nat Rev Neurosci 12:388-399.

11. Ponomarev ED, Maresz K, Tan Y, Dittel BN (2007) CNS-derived interleukin-4 is essential for the regulation of autoimmune inflammation and induces a state of alternative activation in microglial cells. J Neurosci 27:10714-10721.

12. Bradbury EJ, Moon LD, Popat RJ, King VR, Bennett GS, Patel PN, Fawcett JW, McMahon SB (2002) Chondroitinase ABC promotes functional recovery after spinal cord injury. Nature 416:636-640.

13. Frischknecht R, Heine M, Perrais D, Seidenbecher CI, Choquet D, Gundelfinger ED (2009) Brain extracellular matrix affects AMPA receptor lateral mobility and short-term synaptic plasticity. Nat Neurosci 12:897-904.

14. Uchimura K, Kadomatsu K, El-Fasakhany FM, Singer MS, Izawa M, Kannagi R, Takeda N, Rosen SD, Muramatsu T (2004) N-acetylglucosamine 6-O-sulfotransferase-1 regulates expression of L-selectin ligands and lymphocyte homing. J Biol Chem 279:35001-35008.

15. Zhang H, Muramatsu T, Murase A, Yuasa S, Uchimura K, Kadomatsu K (2006) N-Acetylglucosamine 6-O-sulfotransferase-1 is required for brain keratan sulfate biosynthesis and glial scar formation after brain injury. Glycobiology 16:702-710.

16. Ito Z, Sakamoto K, Imagama S, Matsuyama Y, Zhang H, Hirano K, Ando K, Yamashita T, Ishiguro N, Kadomatsu K (2010) N-acetylglucosamine 6-O-sulfotransferase-1-deficient mice show better functional recovery after spinal cord injury. J Neurosci 30:5937-5947.

17. Imagama S, Sakamoto K, Tauchi R, Shinjo R, Ohgomori T, Ito Z, Zhang H, Nishida Y, Asami N, Takeshita S, Sugiura N, Watanabe H, Yamashita T, Ishiguro N, Matsuyama Y, Kadomatsu K (2011) Keratan sulfate restricts neural plasticity after spinal cord injury.

1 J Neurosci 31:17091-17102.

2

3 18. Shen Y, Tenney AP, Busch SA, Horn KP, Cuascut FX, Liu K, He Z, Silver J,

4 Flanagan JG (2009) PTPsigma is a receptor for chondroitin sulfate proteoglycan, an

5 inhibitor of neural regeneration. Science 326:592-596.

6

7 19. Dickendesher TL, Baldwin KT, Mironova YA, Koriyama Y, Raiker SJ, Askew KL,

8 Wood A, Geoffroy CG, Zheng B, Liepmann CD, Katagiri Y, Benowitz LI, Geller HM,

9 Giger RJ (2012) NgR1 and NgR3 are receptors for chondroitin sulfate proteoglycans.

10 Nat Neurosci 15:703-712.

11

12 20. Mizuno H, Warita H, Aoki M, Itoyama Y (2008) Accumulation of chondroitin

13 sulfate proteoglycans in the microenvironment of spinal motor neurons in amyotrophic

14 lateral sclerosis transgenic rats. J Neurosci Res 86:2512-2523.

15

16 21. Vargas MR, Pehar M, Díaz-Amarilla PJ, Beckman JS, Barbeito L (2008)

17 Transcriptional profile of primary astrocytes expressing ALS-linked mutant SOD1. J

18 Neurosci Res 86:3515-3525.

19

20 22. Rolls A, Shechter R, London A, Segev Y, Jacob-Hirsch J, Amariglio N, Rechavi G,

21 Schwartz M (2008) Two faces of chondroitin sulfate proteoglycan in spinal cord repair:

22 a role in microglia/macrophage activation. PLoS Med 5:e171. Available:

23 http://dx.doi.org/10.1371/journal.pmed.0050171. Accessed 19 August 2008.

24

25 23. Shechter R, Raposo C, London A, Sagi I, Schwartz M (2011) The glial

26 scar-monocyte interplay: a pivotal resolution phase in spinal cord repair. PLoS One

27 6:e27969. Available: doi:10.1371/journal.pone.0027969. Accessed 21 December 2011.

28

29 24. Takeuchi H, Mizoguchi H, Doi Y, Jin S, Noda M, Liang J, Li H, Zhou Y, Mori R,

30 Yasuoka S, Li E, Parajuli B, Kawanokuchi J, Sonobe Y, Sato J, Yamanaka K, Sobue G,

31 Mizuno T, Suzumura A (2011) Blockade of gap junction hemichannel suppresses

32 disease progression in mouse models of amyotrophic lateral sclerosis and Alzheimer's

33 disease. PLoS One 6:e21108. Available: doi:10.1371/journal.pone.0021108. Accessed

34 21 June 2011.

35

36 25. Klivenyi P, Ferrante RJ, Matthews RT, Bogdanov MB, Klein AM, Andreassen OA,

1 Mueller G, Wermer M, Kaddurah-Daouk R, Beal MF (1999) Neuroprotective effects of
2 creatine in a transgenic animal model of amyotrophic lateral sclerosis. Nat Med
3 5:347-350.

4

5

1 **Figure legends**

2 **Figure 1**

3 **KS expression was induced in the spinal cords of SOD1^{G93A} mice at end stage.**

4 (A) Lumbar spinal cord lysates (24 weeks of age) were subjected to immunoblotting

5 using anti-KS antibody (5D4) (n=5). β-actin was used as the internal loading control.

6 (B) Lumber spinal cord sections obtained from SOD1^{G93A} mice and their age-matched

7 non-Tg littermates were stained with anti-KS antibody. The lower panels are the highly

8 magnified images of the regions marked with squares. Bars, 200 μm in upper panels; 50

9 μm in lower panels.

10

11 **Figure 2**

12 **KS expression began before body weight loss.**

13 (A) The lysates of the SOD1^{G93A} lumbar spinal cords at 6, 12, 18, and 24 weeks of age

14 were subjected to immunoblotting using the anti-KS antibody 5D4. β-actin was used as

15 the internal loading control. A faint expression of KS was detected at 12 weeks. (B) The

16 SOD1^{G93A} lumber spinal cord section at 12 weeks was stained by anti-KS antibody. KS

17 immunoreactivity was observed in the ventral horn. Bar, 200 μm.

18

1 **Figure 3**

2 **KS was expressed in a subpopulation of microglia.**

3 (A-I) The SOD1^{G93A} mice lumbar spinal cords at 18 weeks were stained by anti-KS (B,

4 E, H), anti-Iba1 (microglia marker; A-C), anti-GFAP (astrocyte marker; D-F), and

5 anti-NG2 (oligodendrocyte precursor marker; G-I) antibodies. Merged images are

6 shown in C, F and I. Bars, 50 μm. Arrows, KS^{+}Iba1^{+} cells; arrowheads, KS^{-}Iba1^{+} cells.

7 (J) A representative profile of KS expression in CD11b^{+} cells. The red line indicates a

8 negative control that does not contain the primary antibody, and the blue line indicates a

9 stained sample. (K) The quantitative data of mean fluorescence intensity (MFI) of KS

10 (n=3). Error bars, SE. **p<0.01. N.S., not significant. (L) The biosynthesis of KS. (M)

11 mRNA expression of the enzymes involved in KS biosynthesis was examined by

12 quantitative RT-PCR using SOD1^{G93A} (gray columns) and their age-matched non-Tg

13 (white columns) mice at 24 weeks. GAPDH was used as the internal control. Error bars,

14 SE. ** p<0.01, * p<0.05 (n=4). N.S., not significant.

15

16 **Figure 4**

17 **KS expression was detected in human ALS.**

18 Human ALS spinal cord sections were stained by anti-Iba1 (A) and anti-KS antibodies

1 (B). Arrows, Iba1$^+$KS$^+$ cells. Bars, 50 μm. The morphology of microglia was confirmed

2 as anti-Iba1 antibody and DAB staining (D). The information of human ALS samples is

3 shown in Figure 4E.

4

5 **Figure 5**

6 **KS expression was attenuated in the SOD1^{G93A}GlcNAc6ST-1$^{-/-}$ mouse spinal cord.**

7 KS expression in the spinal cords of SOD1^{G93A} mice, age-matched non-Tg and

8 SOD1^{G93A}GlcNAc6ST-1$^{-/-}$ mice at 24 weeks was examined by immunoblotting (A) and

9 immunohistochemical (B) analysis. KS was not expressed in the spinal cords of

10 SOD1^{G93A}GlcNAc6ST-1$^{-/-}$ mice. Bars, 200 μm. The number of microglia was examined

11 by immunohistochemical (C) and immunoblotting (D) against Iba1 at 24 weeks. Bars,

12 200 μm. β-actin was used as the internal control (n=4). E, The Iba1 band intensities

13 were quantified by ImageJ. Error bars, SE. **p<0.01. N.S., not significant.

14

15 **Figure 6**

16 **Ablation of KS in microglia accelerated the early phase pathogenesis in a mouse**

17 **model.**

18 (A) The lifespan of SOD1^{G93A} was 164.7±18.2 days (n=43), while that of

1   SOD1^{G93A}GlcNAc6ST-1$^{-/-}$ was 158.7$\pm$13.2 days (n=76) (p=0.007). (B) Body weight

2   loss of SOD1^{G93A} began at 124.7$\pm$12.2 days, while it began at 118.4$\pm$11.9 days in

3   SOD1^{G93A}GlcNAc6ST-1$^{-/-}$ (p=0.005). A decrease in rotarod performance at (C) 15 rpm

4   and (D) 20 rpm of SOD1^{G93A} began at 141.4$\pm$18.2 days and 121.6$\pm$24.5 days,

5   respectively. In SOD1^{G93A}GlcNAc6ST-1$^{-/-}$ mice, these onset times were accelerated to

6   125.2$\pm$14.2 (p<0.001) days and 112.5$\pm$18.1 days (p=0.003), respectively.

7

8   **Figure 7**

9   **A subpopulation of KS-positive microglia was CD86-positive.**

10   The spinal cord sections of SOD1^{G93A} mice at 12, 18 and 24 weeks were stained with

11   KS (A, E, I), M1 marker CD86 (B, F, J), and microglia marker Iba1 (C, G). The merged

12   images are shown in (D, H, K). Arrows, KS$^+$CD86$^+$ microglia; arrowheads, KS$^+$CD86$^-$

13   microglia. Bars, 50 µm. Flow cytometric analysis for CD11b$^+$ cells at 24 weeks.

14   Summaries of CD86 expression (L) and expressions of CD86 and KS (M) are shown.

15   Gray columns, SOD1^{G93A} mice; black columns, SOD1^{G93A}GlcNAc6ST-1$^{-/-}$ mice. Error

16   bars, SE. **p<0.01, *p<0.05 (n=3), N.S., not significance.

17

18   **Figure 8**

1 **Transient enhancement of the expression of M2 markers was diminished in**

2 **SOD1^{G93A}GlcNAc6ST-1$^{-/-}$ mice.**

3 The temporal mRNA expression profiles of M1 [CD86 (A), IL-1β (B), TNF-α (C) and

4 NOX2 (D)] and M2 [Arginase1 (E), CD206 (F), Ym1 (G) and IL-4 (H)] markers were

5 examined by quantitative RT-PCR. Gray columns, SOD1^{G93A} mice; black columns,

6 SOD1^{G93A}GlcNAc6ST-1$^{-/-}$ mice. Error bars, SE. **p$<$0.01, *p$<$0.05 (n=3).

7

8 **Figure 9**

9 **M1 microglia expanded as the disease progressed.**

10 The spinal cord sections of SOD1^{G93A} mice and SOD1^{G93A}GlcNAc6ST-1$^{-/-}$ mice at 15

11 and 24 weeks were stained with KS (A, E, I, M), M1 marker CD86 (B, F, J, N), and

12 microglia marker Iba1 (C, G, K, O). Arrows in A-H, KS^{+}CD86^{+} microglia; arrows in J-P,

13 KS^{-}CD86^{+} microglia; arrowheads, KS^{+}CD86^{-} microglia. Bars, 50 μm.

14

15 **Figure 10**

16 **Expansion of M2 microglia during the early disease phase was suppressed in**

17 **SOD1^{G93A}GlcNAc6ST-1$^{-/-}$ mice.**

18 The spinal cord sections of SOD1^{G93A} mice and SOD1^{G93A}GlcNAc6ST-1$^{-/-}$ mice at 15

1 and 24 weeks were stained with KS (A, E, I, M), M2 marker CD206 (B, F, J, N), and

2 microglia marker Iba1 (C, G, K, O). Arrows, KS⁻CD206⁺ microglia; arrowheads,

3 KS⁺CD206⁻ microglia. Bars, 50 μm.

4

5 **Figure 11**

6 **CD206 was expressed in a subpopulation of microglia distinct from KS+CD86-**

7 **cells.**

8 Sequential thin sections were subjected to immunohistochemical analyses (A). The

9 spinal cord sections of SOD1^{G93A} mice at 15 weeks were stained with KS (B), CD86 (C)

10 and CD206 (D). Arrows, KS⁺CD86⁻ microglia; arrowheads, KS⁻CD206⁺ microglia. Bars,

11 50 μm.

12

1 **Table 1 The primer sequences determined using genotyping of mice**

Target gene	Direction	Primer sequence
SOD1 F	Forward	CATCAGCCCTAATCCATCTGA
	Reverse	CGCGACTAACAATCAAAGTGA
GlcNAc6ST-1 F	Forward	AAGCCTACAGGTGGTGCGAA
	Reverse	CAGGACTGTTAACCCGCTCA
Neo GlcNAc6ST-1	Forward	AGCGTTGGCTACCCGTGATA
	Reverse	GCCAAAAGTGATCACCTCGT
GAPDH	Forward	ACTCACGGCTTCAACG
	Reverse	CCCTGTTGCTGTAGCCGTA

2

3 **Table 2 The primer sequences using quantitative RT-PCR of M1 and M2 markers**

Target gene	Direction	Primer sequence
CD86	Forward	ACGATGGACCCCAGATGCACCA
	Reverse	GCGTCTCCACGGAAACAGCA
IL-1β	Forward	CCTGCAGCTGGAGAGTGTGGAT
	Reverse	TGTGCTCTGCTTGTGAGGTGCT
TNF	Forward	AGCCCACGTCGTAGCAAACCAC
	Reverse	AGGTACAACCCATCGGCTGGCA
NOX2	Forward	TCTCAGGGGTTCCAGTGCGTGT
	Reverse	TGTGGATGGCGGTGTGCAGT
Arginase1	Forward	TTAGGCCAAGGTGCTTGCTGCC
	Reverse	TACCATGGCCCTGAGGAGGTTC
CD206	Forward	TCAGCTATTGGACGCGAGGCA
	Reverse	TCCGGGTTGCAAGTTGCCGT
Ym1	Forward	ACCCCTGCCTGTGTACTCACCT
	Reverse	CACTGAACGGGGCAGGTCCAAA
IL-4	Forward	TGGGTCTCAACCCCCAGCTAGT
	Reverse	TGCATGGCGTCCCTTCTCCTGT

4

K. Hirano et al., Figure 1

Figure2

K. Hirano et al., Figure 2

K. Hirano et al., Figure 3

K. Hirano et al., Figure 4

Human FALS 185

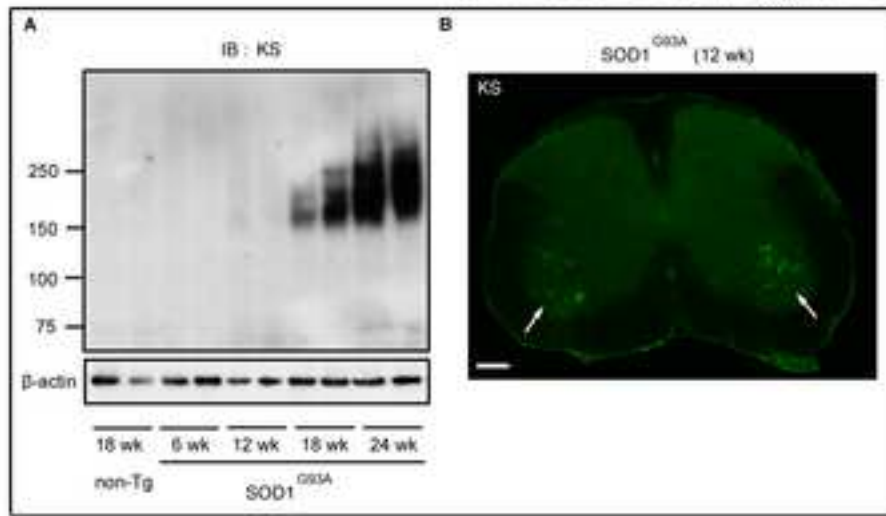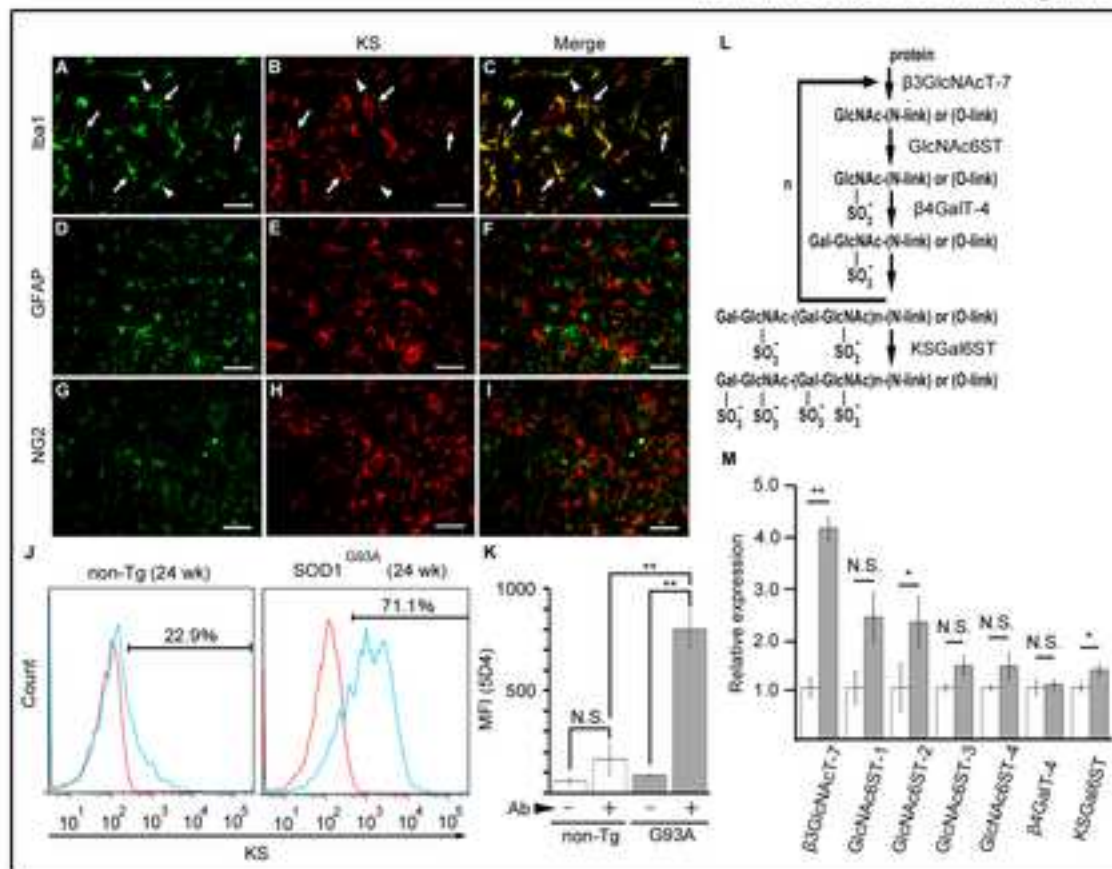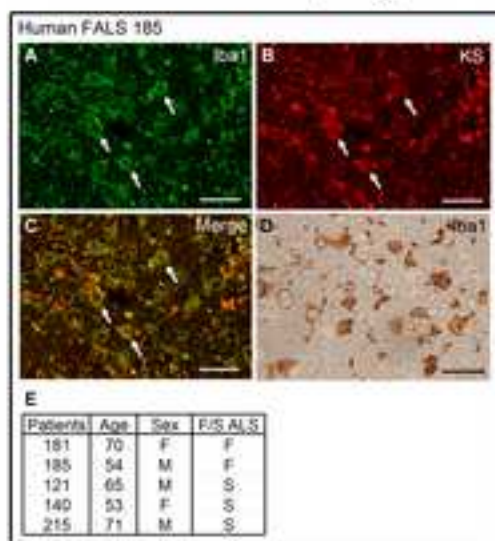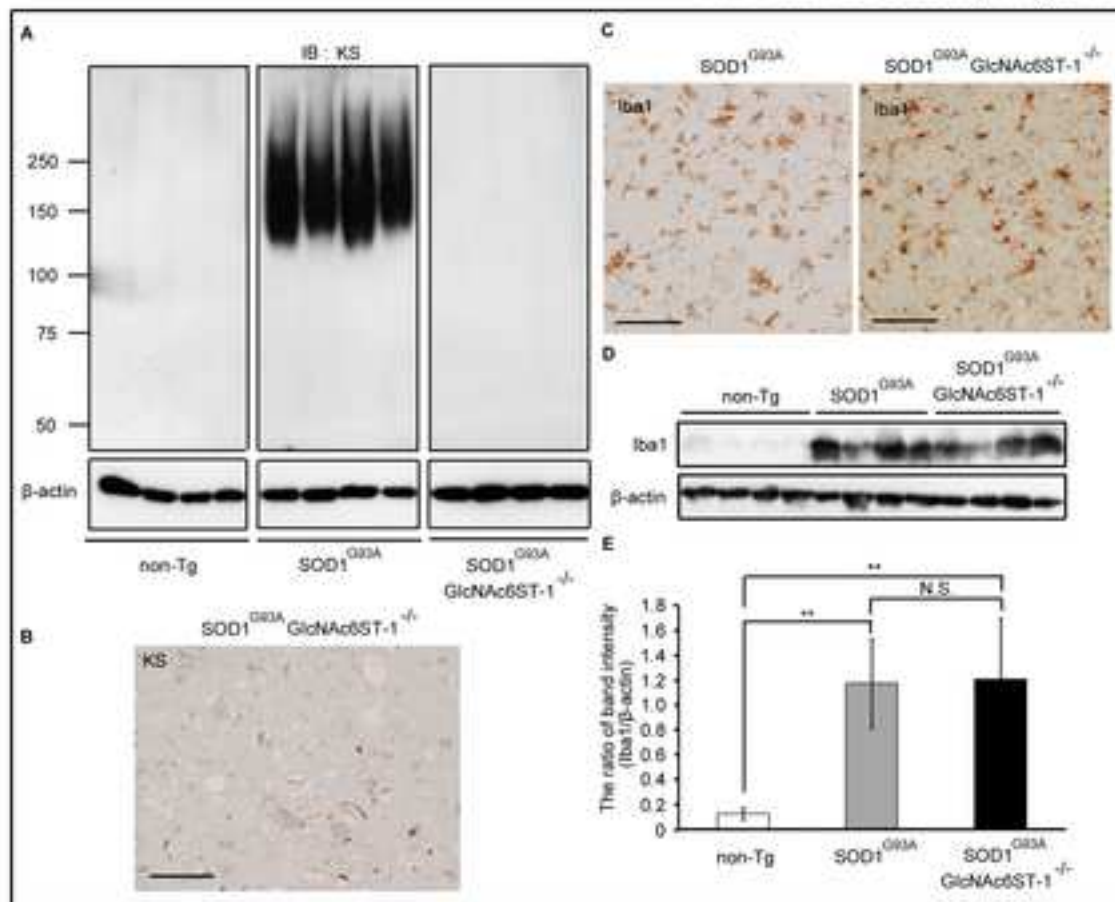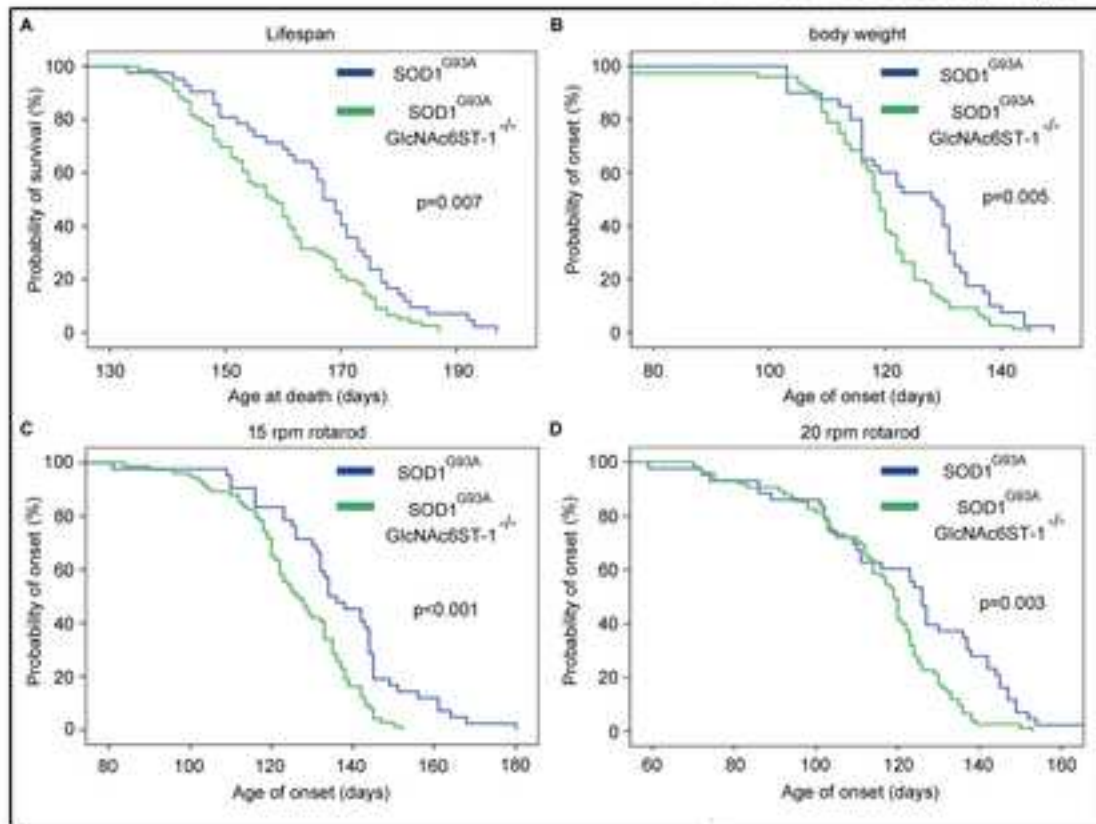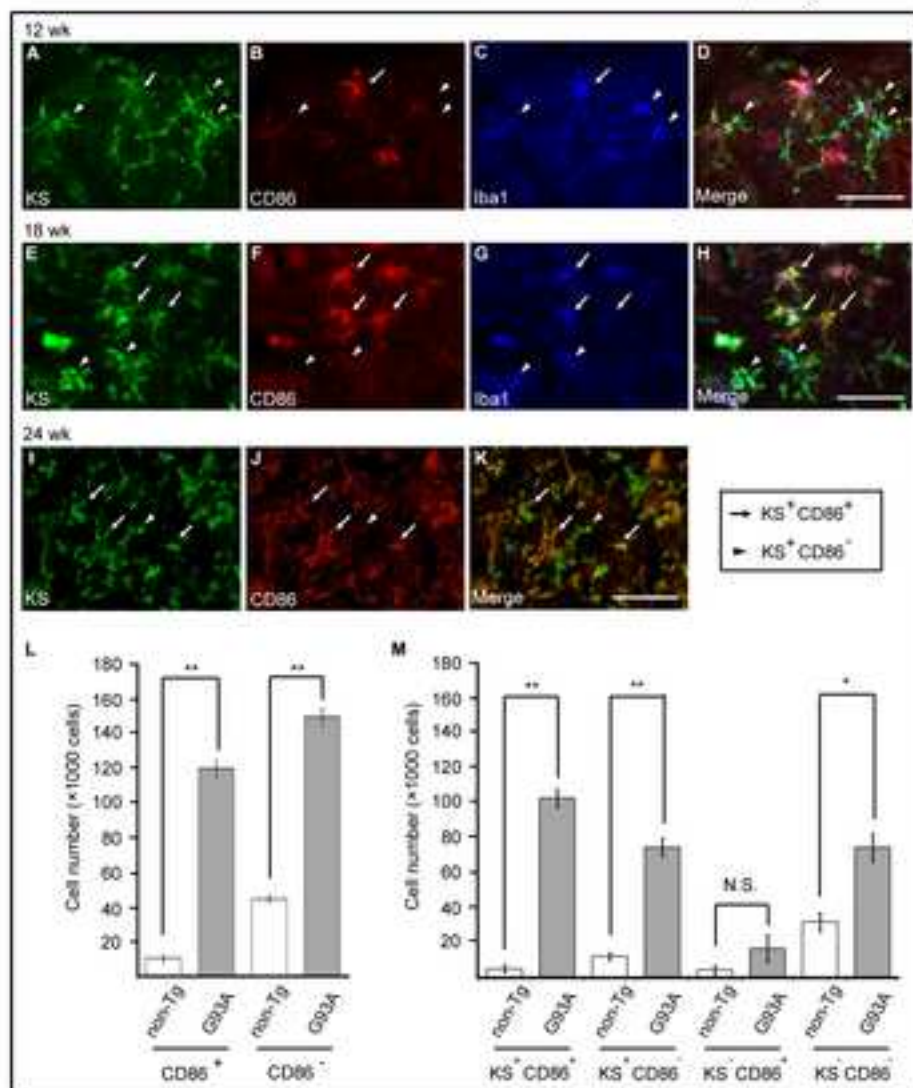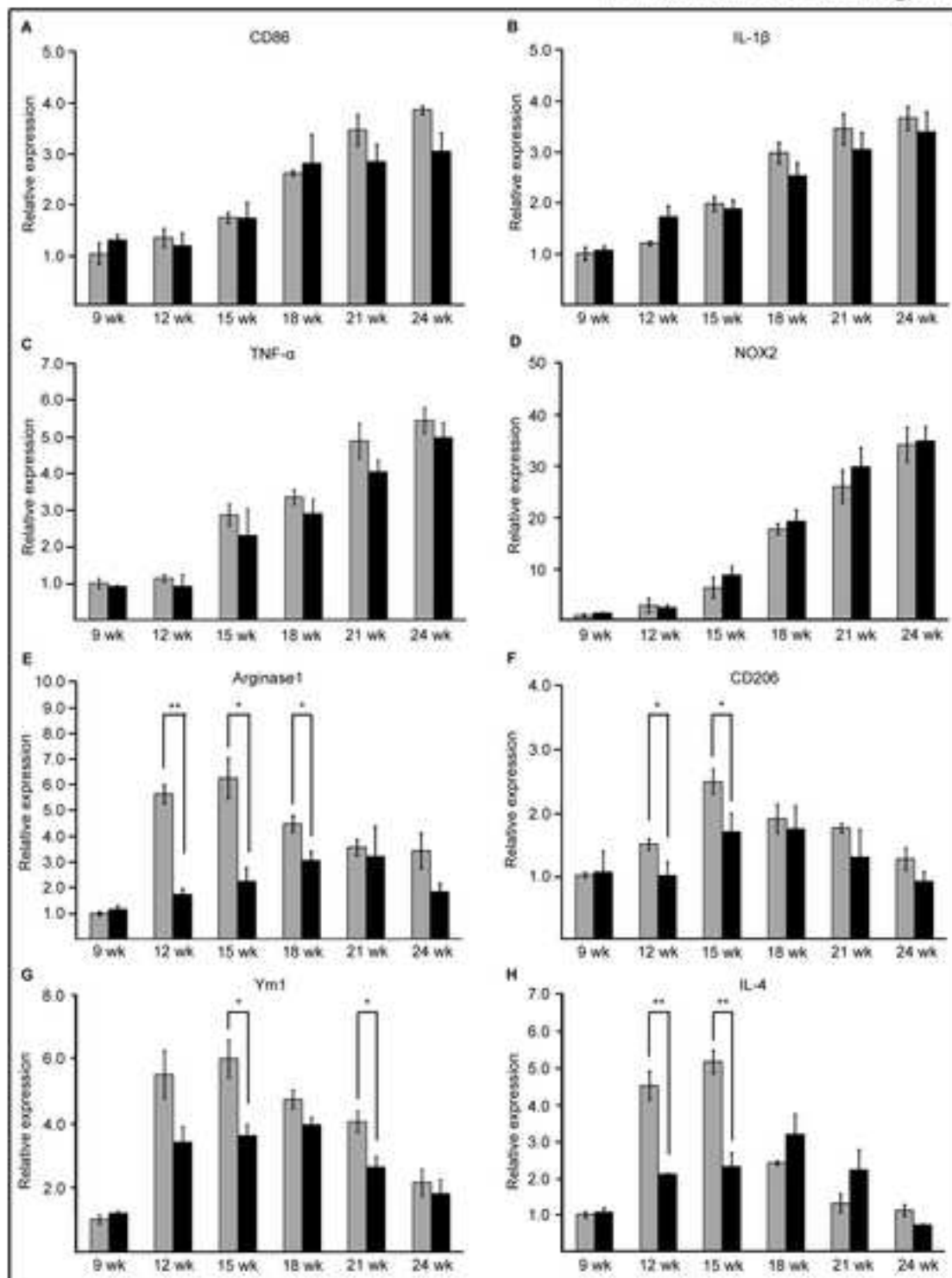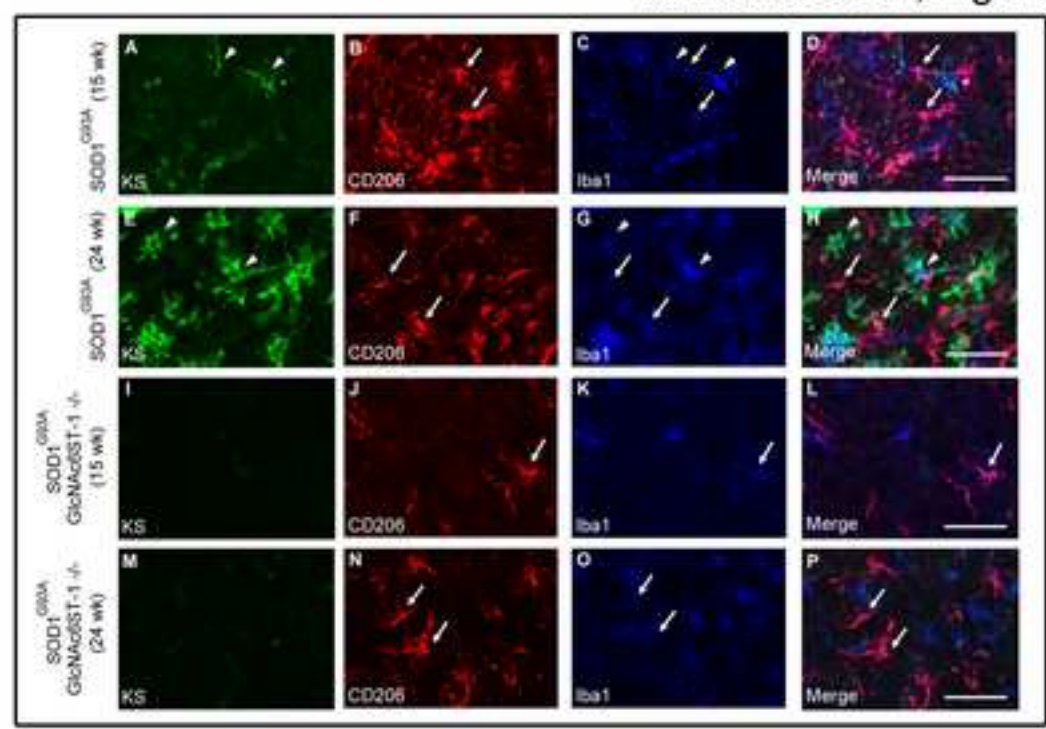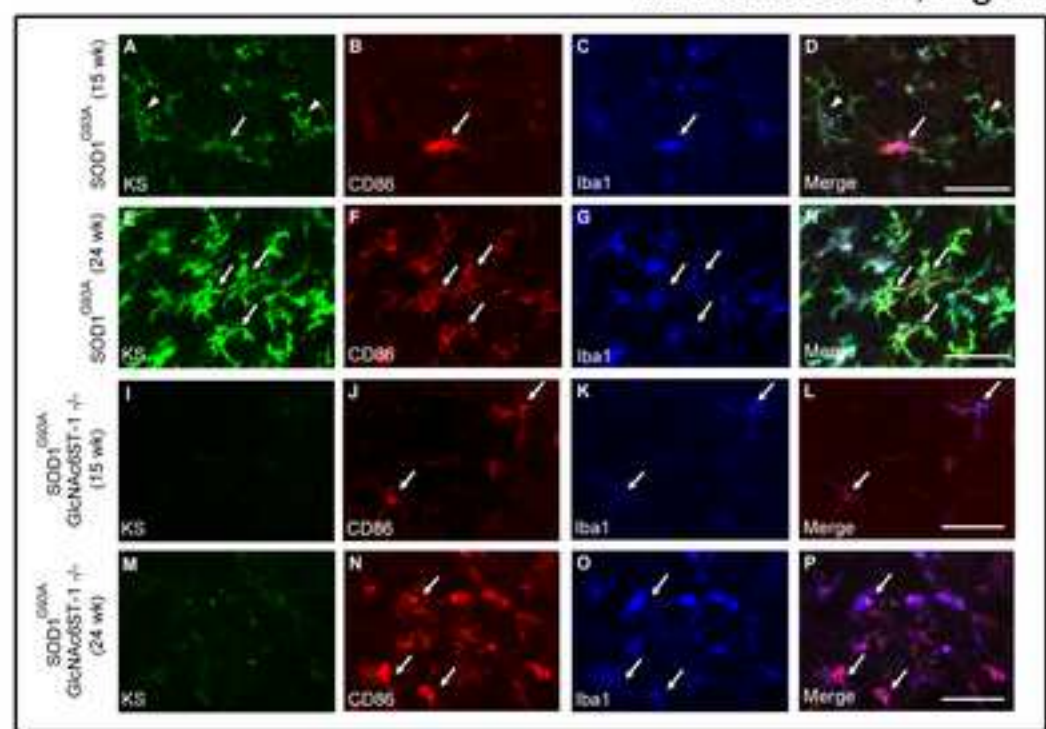| Patients	Age	Sex	F/S ALS
181	70	F	F
185	54	M	F
121	65	M	S
140	53	F	S
215	71	M	S

Figure5
Click here to download high resolution image

K. Hirano et al., Figure 5

K. Hirano et al., Figure 6

K. Hirano et al., Figure 7

K. Hirano et al., Figure 8

Figure10
Click here to download high resolution image

K. Hirano et al., Figure 10

K. Hirano et al., Figure 9

Figure11
Click here to download high resolution image

K. Hirano et al., Figure 11